Spatially resolved Raman analysis of laser induced refractive index variation in chalcogenide glass

Pascal Masselin,* David Le Coq, Arnaud Cuisset, and Eugène Bychkov

Laboratoire de Physico Chimie de l'Atmosphère,
Université du Littoral Cte d'Opale, 59140 Dunkerque, France

*masselin@univ-littoral.fr

Abstract: We report a detailed 2D μ-Raman analysis of the refractive index modification (Δn) induced by femtosecond laser filament in the bulk of Ge-Ga-S ternary chalcogenide glass. The invariant illumination and detection geometry during the 2D scanning, allows both qualitative and quantitative determination of the proportion of different structural units to be carried out. The results indicate that during the light-matter interaction, S_3Ga-GaS_3 ethane like groups are transformed into triclusters of Ga/S. The decreased population of edge- and corner-sharing $GeS_{4/2}$ tetrahedra implies the formation of mixed triclusters : T/S where T = Ga and/or Ge. Finally, correlations between photostructural changes and Δn are presented.

OCIS codes: (140.3390) Laser materials processing; (160.2750) Glass and other amorphous materials; (320.2250) Femtosecond phenomena.

References and links

1. R. R. Gattass and E. Mazur, "Femtosecond laser micromachining in transparent materials," Nat. Photonics **2**, 219–225 (2008).
2. G. D. Valle, R. Osellame, and P. Laporta, "Micromachining of photonic devices by femtosecond laser pulses," J. Opt. A, Pure Appl. Opt. **11**, 013001 (2009).
3. R. Osellame, G. Cerullo, and R. Ramponi, *Femtosecond Laser Micromachining: Photonic and Microfluidic Devices in Transparent Materials*, Topics in Applied Physics (Springer, 2012).
4. L. B. Fletcher, J. J. Witcher, N. Troy, S. T. Reis, R. K. Brow, and D. M. Krol, "Direct femtosecond laser waveguide writing inside zinc phosphate glass," Opt. Express **19**, 7929–7936 (2011).
5. J. W. Chan, T. Huser, S. Risbud, and D. M. Krol, "Structural changes in fused silica after exposure to focused femtosecond laser pulses," Opt. Lett. **26**, 1726–1728 (2001).
6. J. Chan, T. Huser, S. Risbud, and D. Krol, "Modification of the fused silica glass network associated with waveguide fabrication using femtosecond laser pulses," Appl. Phys. A: Mater. Sci. Process. **76**, 367–372 (2003).
7. D. J. Little, M. Ams, P. Dekker, G. D. Marshall, J. M. Dawes, and M. J. Withford, "Femtosecond laser modification of fused silica: the effect of writing polarization on Si-O ring structure," Opt. Express **16**, 20029–20037 (2008).
8. L. B. Fletcher, J. J. Witcher, N. Troy, S. T. Reis, R. K. Brow, R. M. Vazquez, R. Osellame, and D. M. Krol, "Femtosecond laser writing of waveguides in zinc phosphate glasses," Opt. Mat. Express **1**, 845–855 (2011).
9. D. Krol, "Femtosecond laser modification of glass," J. Non-Cryst. Solids **354**, 416–424 (2008).
10. J. D. Musgraves, K. Richardson, and H. Jain, "Laser-induced structural modification, its mechanisms, and applications in glassy optical materials," Opt. Mater. Express **1**, 921–935 (2011).
11. A. Couairon and A. Mysyrowicz, "Femtosecond filamentation in transparent media," Phys. Rep. **441**, 47–189 (2007).
12. P. Masselin, D. Le Coq, E. Bychkov, E. Lepine, C. Lin, and L. Calvez, "Laser filamentation in chalcogenide glass," Proc. SPIE **7993**, 79931B (2010).
13. O. Caulier, D. Le Coq, L. Calvez, E. Bychkov, and P. Masselin, "Free carrier accumulation during direct laser writing in chalcogenide glass by light filamentation," Opt. Express **19**, 20088–20096 (2011).

#172819 - $15.00 USD Received 18 Jul 2012; revised 15 Oct 2012; accepted 20 Oct 2012; published 12 Nov 2012

14. C. Lin, L. Calvez, M. Rozé, H. Tao, X. Zhang, and X. Zhao, "Crystallization behavior of 80 $GeS_2 - 20\ Ga_2S_3$ chalcogenide glass," Appl. Phys. A: Mater. Sci. Process. **97**, 713–720 (2009).
15. D. Le Coq, P. Masselin, A. Cuisset, and E. Bychkov, "Raman spectra of 80 GeS_2 - 20 Ga_2S_3," J. Raman Spectrosc. (in preparation).
16. G. Lucovsky, F. L. Galeener, R. C. Keezer, R. H. Geils, and H. A. Six, "Structural interpretation of the infrared and Raman spectra of glasses in the alloy system $Ge_{1-x}S_x$," Phys. Rev. B **10**, 5134–5146 (1974).
17. H. Takebe, H. Maeda, and K. Morinaga, "Compositional variation in the structure of GeS glasses," J. Non-Cryst. Solids **291**, 14–24 (2001).
18. I. P. Kotsalas and C. Raptis, "High-temperature structural phase transitions of Ge_xS_{1-x} alloys studied by Raman spectroscopy," Phys. Rev. B **64**, 125210 (2001).
19. J. E. Griffiths, J. C. Phillips, G. P. Espinosa, J. P. Remeika, and P. M. Bridenbaugh, "Assignment of the companion A_{1c} line in $GeX(S, Se)_{1-x}$ glasses," Phys. Status Solidi B **122**, K11–K15 (1984).
20. S. Sugai, "Stochastic random network model in Ge and Si chalcogenide glasses," Phys. Rev. B **35**, 1345–1361 (1987).
21. K. Inoue, O. Matsuda, and K. Murase, "Raman spectra of tetrahedral vibrations in crystalline germanium dichalcogenides, GeS_2 and $GeSe_2$, in high and low temperature forms," Solid State Commun. **79**, 905–910 (1991).
22. P. M. Bridenbaugh, G. P. Espinosa, J. E. Griffiths, J. C. Phillips, and J. P. Remeika, "Microscopic origin of the companion A_1 Raman line in glassy $Ge(S, Se)_2$," Phys. Rev. B **20**, 4140–4144 (1979).
23. K. Jackson, A. Briley, S. Grossman, D. V. Porezag, and M. R. Pederson, "Raman-active modes of $a-GeSe_2$ and $a-GeS_2$: a first-principles study," Phys. Rev. B **60**, R14985–R14989 (1999).
24. S. Blaineau and P. Jund, "Vibrational signature of broken chemical order in a GeS_2 glass: A molecular dynamics simulation," Phys. Rev. B **69**, 064201 (2004).
25. A. Tverjanovich, Y. Tveryanovich, and S. Loheider, "Raman spectra of gallium sulfide based glasses," J. Non-Cryst. Solids **208**, 49–55 (1996).
26. T. Haizheng, Z. Xiujian, J. Chengbin, and L. Sheng, "Microstructural probing of (1-x) GeS_2 - x Ga_2S_3 system glasses by Raman scattering," J. Wuhan Univ. Technol. **20**, 8–10 (2005).
27. Y. Ledemi, S. Messaddeq, I. Skhripachev, S. Ribeiro, and Y. Messaddeq, "Influence of Ga incorporation on photoinduced phenomena in GeS based glasses," J. Non-Cryst. Solids **355**, 1884–1889 (2009).
28. C. Lin, L. Calvez, H. Tao, M. Allix, A. Moréac, X. Zhang, and X. Zhao, "Evidence of network demixing in $GeS_2 - Ga_2S_3$ chalcogenide glasses: a phase transformation study," J. Solid State Chem. **184**, 584–588 (2011).
29. A. Cuisset, F. Hindle, J. Laureyns, and E. Bychkov, "Structural analysis of xCsCl $-(1-x)Ga_2S_3$ glasses by means of DFT calculations and Raman spectroscopy," J. Raman Spectrosc. **41**, 1050–1058 (2010).
30. M. J. Frisch, G. W. Trucks, H. B. Schlegel, G. E. Scuseria, M. A. Robb, J. R. Cheeseman, J. A. Montgomery Jr., T. Vreven, K. N. Kudin, J. C. Burant, J. M. Millam, S. S. Iyengar, J. Tomasi, V. Barone, B. Mennucci, M. Cossi, G. Scalmani, N. Rega, G. A. Petersson, H. Nakatsuji, M. Hada, M. Ehara, K. Toyota, R. Fukuda, J. Hasegawa, M. Ishida, T. Nakajima, Y. Honda, O. Kitao, H. Nakai, M. Klene, X. Li, J. E. Knox, H. P. Hratchian, J. B. Cross, C. Adamo, J. Jaramillo, R. Gomperts, R. E. Stratmann, O. Yazyev, A. J. Austin, R. C. Cammi, Pomelli, J. W. Ochterski, P. Y. Ayala, K. Morokuma, G. A. Voth, P. Salvador, J. J. Dannenberg, V. G. Zakrzewski, S. Dapprich, A. D. Daniels, M. C. Strain, O. Farkas, D. K. Malick, A. D. Rabuck, K. Raghavachari, J. B. Foresman, J. V. Ortiz, Q. Cui, A. G. Baboul, S. Clifford, J. Cioslowski, B. B. Stefanov, G. Liu, A. Liashenko, P. Piskorz, I. Komaromi, R. L. Martin, D. J. Fox, T. Keith, M. A. Al-Laham, C. Y. Peng, A. Nanayakkara, M. Challacombe, P. M. W. Gill, B. Johnson, W. Chen, M. W. Wong, C. Gonzalez, and J. A. Pople, "Gaussian 03, Revision B. 04," (Gaussian, Inc., Pittsburgh, PA., 2003).
31. A. D. Becke, "Density-functional thermochemistry. iii. the role of exact exchange," J. Chem. Phys. **98**, 5648–5652 (1993).
32. C. Lee, W. Yang, and R. G. Parr, "Development of the Colle-Salvetti correlation-energy formula into a functional of the electron density," Phys. Rev. B . **37**, 785–789 (1988).
33. D. Long, *Raman Spectroscopy* (McGraw-Hill, 1977).
34. M. J. Pelletier, "Quantitative analysis using Raman spectrometry," Appl. Spectrosc. **57**, 20A–42A (2003).
35. E. Ampem-Lassen, S. T. Huntington, N. M. Dragomir, K. A. Nugent, and A. Roberts, "Refractive index profiling of axially symmetric optical fibers: a new technique," Opt. Express **13**, 3277–3282 (2005).
36. A. Mermillod-Blondin, I. M. Burakov, Y. P. Meshcheryakov, N. M. Bulgakova, E. Audouard, A. Rosenfeld, A. Husakou, I. V. Hertel, and R. Stoian, "Flipping the sign of refractive index changes in ultrafast and temporally shaped laser-irradiated borosilicate crown optical glass at high repetition rates," Phys. Rev. B **77**, 104205 (2008).
37. J. Canning, M. Lancry, K. Cook, A. Weickman, F. Brisset, and B. Poumellec, "Anatomy of a femtosecond laser processed silica waveguide," Opt. Mater. Express **1**, 998–1008 (2011).
38. L. Sudrie, A. Couairon, M. Franco, B. Lamouroux, B. Prade, S. Tzortzakis, and A. Mysyrowicz, "Femtosecond laser-induced damage and filamentary propagation in fused silica," Phys. Rev. Lett. **89**, 186601 (2002).
39. S. Eaton, H. Zhang, P. Herman, F. Yoshino, L. Shah, J. Bovatsek, and A. Arai, "Heat accumulation effects in femtosecond laser-written waveguides with variable repetition rate," Opt. Express **13**, 4708–4716 (2005).

#172819 - $15.00 USD Received 18 Jul 2012; revised 15 Oct 2012; accepted 20 Oct 2012; published 12 Nov 2012

1. Introduction

Direct laser writing is now a well known technique to induce very localized refractive index variation (Δn) in various materials [1, 2] including polymers, crystals and glasses, and it has been applied successfully to produce passive and active photonic devices [3].

However, the result of the light-matter interaction in term of Δn is still not predictable and thus the required photoinscription parameters are determined empirically from systematic studies. As an example, small changes in the glass composition can lead to positive Δn (and then guiding) or to negative Δn [4]. Then it is needed to understand the structural modifications of the glass that cause a positive or negative Δn.

Several studies have been carried out in this sense on various glasses. In particular, a higher concentration of 3-member rings has been observed in silicate glasses after femtosecond pulse irradiation with corresponding decrease of 4-member rings population. The resulting glass densification leads to a positive Δn [5–7]. In the case of zinc phosphate glass, the interaction causes the depolymerisation of the glass network [8]. For a review, the reader can refer to [9, 10].

Our study is focused on the glass network modification of ternary chalcogenide glass ($80\ GeS_2 - 20\ Ga_2S_3$) by femtosecond laser pulses in order to find the correlation with induced refractive index changes. Since chalcogenide glass are highly nonlinear, the laser beam experiences self-focusing and a light filament can easily be formed [11]. This particular condition of light propagation leads to Δn having a spatial extension along the beam propagation direction much longer than the Rayleigh length [12]. The resulting structure can have only positive Δn regions [13] or more complex features with negative and positive parts [12], depending on the repetition rate of the laser.

In our study, a 2D $\mu-$Raman mapping of the region modified by the laser pulses is realized and the reorganization of chemical bonds is evidenced. The contribution to the Raman signal from each structural unit that composes the glass network, is determined in all the points of the mapping. Quantitative analysis of every contribution over more than 11,000 spectra is allowed by the constant detection conditions during the 2D scanning of the sample.

2. Experiments

The experiment consists in a static irradiation of $80\ GeS_2 - 20\ Ga_2S_3$ glass and a 2D Raman mapping of the resulting Δn.

The light source used in the experiment is a high repetition rate (76 MHz) femtosecond Ti:Sa laser (Mira Coherent Inc.) delivering pulse of duration around $\sim$200 fs, 2.6 nJ energy and a central wavelength of 800 nm. The beam is focused in the bulk of the sample by a X5 (0.1 NA) microscope objective. The glass irradiation is performed in static conditions (without sample translation) and the exposure duration is set to 1 second. Further information on the writing procedure are given in [12] and the glass preparation is detailed in [14].

After the irradiation the sample is cleaved to bring the irradiated area near the surface. Raman spectra are recorded using a Jobin-Yvon Raman micro-spectrometer with a X100 objective. A He-Ne laser ($\lambda = 632$ nm) was used as excitation source. The laser power was limited to 1 mW to avoid the laser damage of the sample surface. The sample is translated with a resolution of 1 μm in the direction perpendicular to the beam propagation direction and 2 μm in the beam direction, to obtain a complete Δn mapping dimensions $326 \times 68\ \mu m^2$. A special attention was paid to the sample alignement to ensure an invariant illumination and detection geometry.

#172819 - $15.00 USD Received 18 Jul 2012; revised 15 Oct 2012; accepted 20 Oct 2012; published 12 Nov 2012

3. Results and discussion

3.1. Fitting procedure

The main idea of the fitting is to identify contributions of different structural groups to the Raman spectra of the non-irradiated glass and to observe their evolutions in the irradiated zone along with the 2D scan. Direct qualitative and quantitative comparison between the spectra appears to be possible because the geometric factor, solid angle seen by the detector, detector efficiency are the same. The invariant detection conditions have been confirmed by the reproducibility between the spectra of non-irradiated matrix obtained for different positions.

In this paper we do not present a complete analysis of Ge-Ga-S glass structure that will be published elsewhere [15]. We are interested in the 2D evolution of the contribution from different structural groups. The groups to be considered are determined starting from a comparison of the Raman spectra of 80 GeS_2 − 20 Ga_2S_3 and 10 GeS − 90 GeS_2 glasses, as given in the Fig. 1.

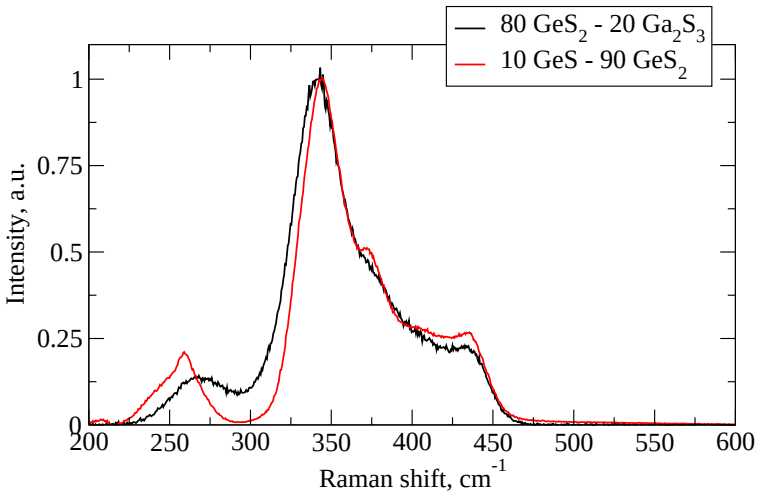

Fig. 1. Raman spectra of the 80 GeS_2 − 20 Ga_2S_3 and 10 GeS − 90 GeS_2 glasses.

The Ge-rich binary glass exhibits usual spectroscopic features for the g-Ge_xS_{100-x} glassy system at $x > 33.3$ (see for example [16–18] and references therein). The most intense line at 344 cm^{-1} correspond to A_1 symmetric in-phase breathing of corner-sharing CS-$GeS_{4/2}$ tetrahedra [19–21], accompanied by an A_{1c} companion line at 372 cm^{-1} [22] related to symmetric breathing of edge-sharing ES-$GeS_{4/2}$ units [20,21]. The broad asymmetric feature at 259 cm^{-1} originates from Ge-Ge vibrations in S_3Ge-GeS_3 ethane like units [16, 18, 23]. Recent *ab initio* calculations [23, 24] have shown that the broad poorly resolved feature around 400 cm^{-1} contains contributions from both CS and ES tetrahedra, but the peaks at 436 cm^{-1} is due entirely to the highest mode in the ES tetrahedra [24].

Surprisingly, the stoichiometric 80 GeS_2 − 20 Ga_2S_3 glass exhibits rather similar Raman spectrum to the Ge-rich binary composition. As difference we note (i) a blue shift of the low frequency feature from 259 to 268 cm^{-1}, (ii) an asymmetric broadening of the A_1 line at low frequencies, and (iii) some decrease of the intensity of the vibration modes corresponding to ES-$GeS_{4/2}$ units , i.e., at 372 cm^{-1} (A_{1c} mode) and 436 cm^{-1}. Similar changes were reported earlier for related Ga-Ge-S glasses compared to the Ge-S parents [25–28].

Since Ge and Ga have nearly the same atomic masses, the band at 268 cm^{-1} indicates that

#172819 - $15.00 USD Received 18 Jul 2012; revised 15 Oct 2012; accepted 20 Oct 2012; published 12 Nov 2012

80 GeS_2 − 20 Ga_2S_3 glass should contain S_3Ga-GaS_3 and/or S_3Ge-GaS_3 ethane like units. However, pure Ge ethane like contribution seems to be unlikely in 80 GeS_2 − 20 Ga_2S_3 while the Ge-Ge vibrational mode appears only in Ge-rich compositions of g-Ge_xS_{100-x} glass ($x >$ 33.3).

Taking into account the four-fold coordination of Ga [27] and the Ga_2S_3 stoichiometry, sulfur should exist in two- and three-fold coordination environments, i.e., as $\left[GaS_{1/3}S_{3/p}\right]_3$ tetrahedral triclusters where $p = 2,3$. Such tricluster contribution to the Raman spectra was found earlier for CsCl-Ga_2S_3 glass [29].

Consequently, the calculations performed in this study target four structural units: CS-$GeS_{4/2}$, ES-$GeS_{4/2}$, S_3Ga-GaS_3 ethane like units and $\left[GaS_{1/3}S_{3/p}\right]_3$ ($p = 2,3$) triclusters.

Theoretical calculations are performed using GAUSSIAN 03 [30] associated with its graphical user interface GaussView 03. In order to find a compromise between the cost of the calculations and the accuracy of the results, structural optimisations and harmonic vibrational frequency calculations are performed for size-limited clusters composed of $Ga(SH)_4$ and $Ge(SH)_4$ tetrahedral subunits. Calculations on $Ga(SH)_4$ clusters are described in details in Ref. [29]. In this study, density functional theory (DFT) harmonic frequency calculations for the Raman active vibrations of S_3Ga-GaS_3 ethane like group and tricluster formed of Ga/S are re-examined. DFT calculations are performed with the Becke [31] three parameters hybrid exchange func-

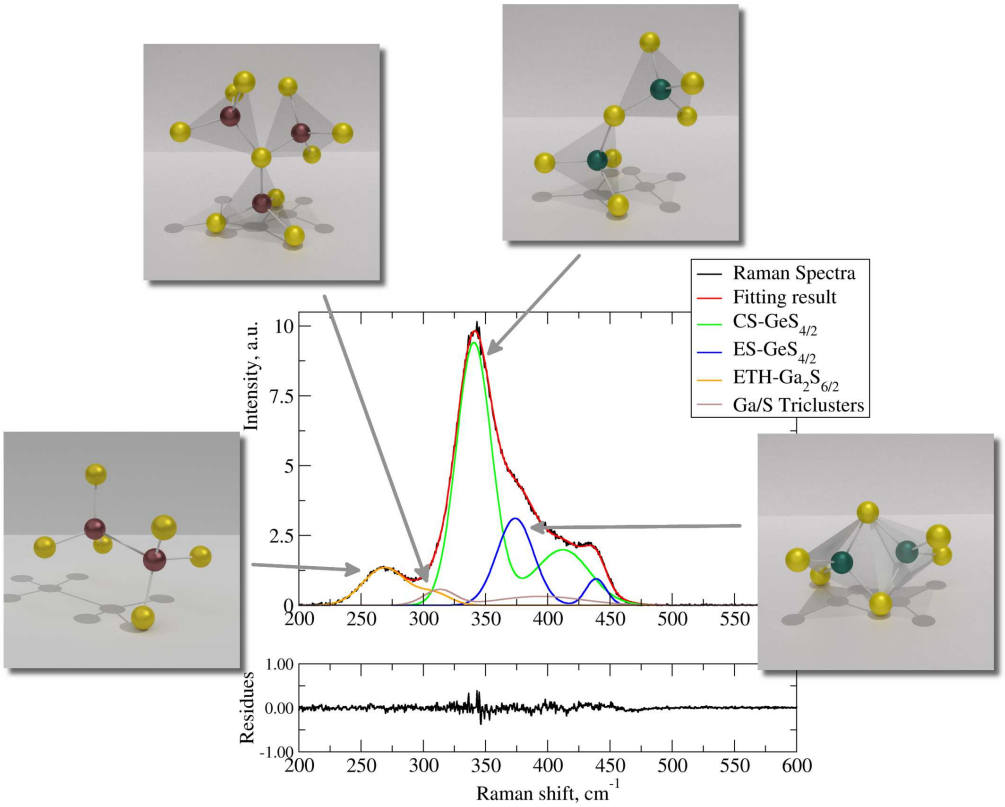

Fig. 2. Raman spectra of the 80 GeS_2 − 20 Ga_2S_3 glass and the result of the fit. The contributions of each group are shown by the colored line. Residues are also shown on the bottom. An artist view of each structural group highlights the well-resolved contribution of the group.

#172819 - $15.00 USD Received 18 Jul 2012; revised 15 Oct 2012; accepted 20 Oct 2012; published 12 Nov 2012

tional and the Lee-Yang-Parr correlation functional (B3LYP) [32]. All the structures are optimised using the GDIIS convergence criteria ensuring adequate convergence and reliability of computed wavenumbers. Harmonic frequency calculations are performed with the method and basis set used for the optimisation. Using the 6-311G+(2d,p) basis set, the best quality of the wavenumber predictions is obtained with an optimum scaling factor close to 1 and a root-mean square standard deviation around 5 cm^{-1} [29]. In order to obtain similar accuracies for the GeS_4 tetrahedron edge-sharing (ES) and corner-sharing (CS) dimers harmonic frequencies, an extension to the 6-311G++(3df,2p) basis set is required.

In the fitting procedure, every vibrational mode determined by the DFT calculations is represented by a Gaussian function. The non-irradiated glass (matrix) spectra has been fitted by fixing the frequency and the relative intensity of each vibration mode inside a group, according to the result of DFT calculation. The varying parameters are the Gaussian full width at half maximum and the relative amplitude of the contributions of the four groups. In Fig. 2 the Raman spectrum of the matrix and the fitting results are presented together with the residues.

It can be seen in this figure that every group has a characteristic well resolved vibration mode from which the behaviour of the contribution of the groups can unambiguously be determined. The low frequency band centered at 275 cm^{-1} is due to S_3Ga-GaS_3 ethane like group (ETH-$Ga_2S_{6/2}$). The edge sharing GeS_4 tetrahedron (ES-$GeS_{4/2}$) has a signature at 376 cm^{-1} while the more intense peak at 341 cm^{-1} is a contribution from the corner sharing tetrahedron (CS-$GeS_{4/2}$). The tricluster of tetrahedra possesses a marked contribution between the ETH and the CS bands and a larger one between 350 and 450 cm^{-1}.

Consequently, the contribution of each group in the Raman spectra is clearly identified in the spectra of the non-irradiated matrix. Then a complete mapping of the entire region is obtained by fitting the spectra in each point with only four relative amplitude of each contribution as fitting parameter. We note that for all the spectra, the R^2 coefficient changes between 0.9980 and 0.9996.

3.2. Raman mapping results

In Fig. 3, the mapping of the four contributions are shown. All the amplitudes are normalized to the mean value of the matrix. The influence of the femtosecond pulse is clearly seen on all contributions. On this figure, the laser beam propagates from the left to the right.

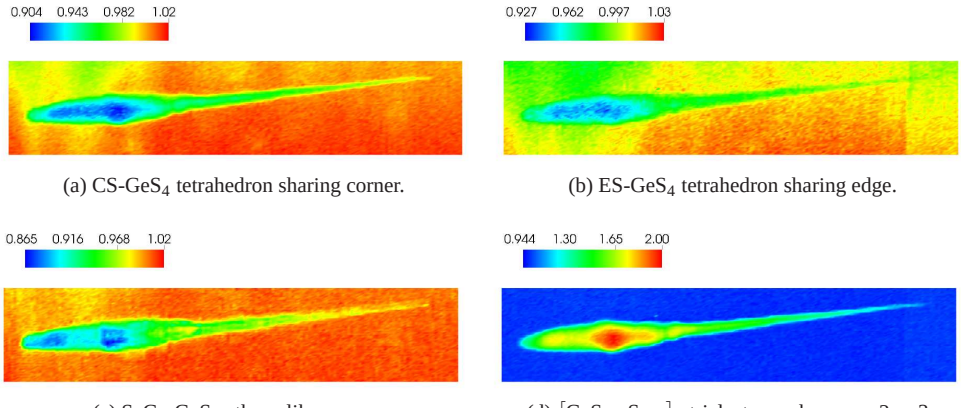

(a) CS-GeS_4 tetrahedron sharing corner.

(b) ES-GeS_4 tetrahedron sharing edge.

(c) S_3Ga-GaS_3 ethane like group

(d) $\left[GaS_{1/3}S_{3/p}\right]_3$ triclusters, where $p = 2$ or 3.

Fig. 3. Mapping of the relative contribution of the four groups into the Raman spectra.

#172819 - $15.00 USD Received 18 Jul 2012; revised 15 Oct 2012; accepted 20 Oct 2012; published 12 Nov 2012

First, the fs-laser irradiation increases the tricluster population and decreases the fraction of S_3Ga-GaS_3 ethane-like units, (see Figs. 3d and 3c). We should note that this trend is observed for both positive and negative Δn regions (see Fig. 4b); however the magnitude of changes are distinctly different. Regions with the highest $|\Delta n|$ changes (called hereafter the head) are characterised by a two-fold increase of triclusters, while the tricluster fraction in the positive Δn domains (called hereafter the tail) does not exceed $+30-40\%$ compared to the non-irradiated matrix (see Fig. 4b). The tricluster formation is not just a conversion of S_3Ga-GaS_3 ethane-like units into triclusters. The related changes in the S_3Ga-GaS_3 population are significantly smaller (-15%) compared to triclusters ($+100\%$). However, the decrease of the CS- and ES-GeS_4 population is consistent with the formation of mixed triclusters $\left[TS_{1/3}S_{3/p}\right]_3$ where $p=2$ or 3, and T = Ga and/or Ge, Figs. 3a and 3b.

3.3. Correlation with the refractive index variation

The intensity of the Raman scattered light is proportional to the number of scattering units, N, in the sample volume being probed by the Raman instrument [33, 34]. In our conditions of identical instrument efficiency and geometric factor, the enhanced or reduced Raman integrated intensity reflects the increased average number density in sample regions with $\Delta n > 0$ or the diminished average number density for regions with $\Delta n < 0$.

In the Fig. 4 we compare the mapping of Δn and the integrated Raman intensity, and also a photography of Δn (Fig. 4a). The Δn mapping (Fig. 4b) is obtained by quantitative phase imaging followed by an Abel inversion [35]. This procedure can be used if Δn possess an axial symmetry and it results in a $\Delta n(r,y)$ where r is the distance to symmetry axis. Therefore the image 4b has an other meaning than the Fig. 4c where the Raman mapping is represented in the (x,y) plane. This mapping represents the total intensity of the Raman signal in each point.

It is clear from these two figures that an increase of the refractive index is associated to an increase of the Raman signal while a negative Δn is related to a decrease of the Raman intensity. Positive refractive index changes are closely related to the tricluster population simply because the efficient packing of triclusters gives higher density and number density, thus increasing the refractive index. Crystalline references clearly show the effect of triclusters on network densi-

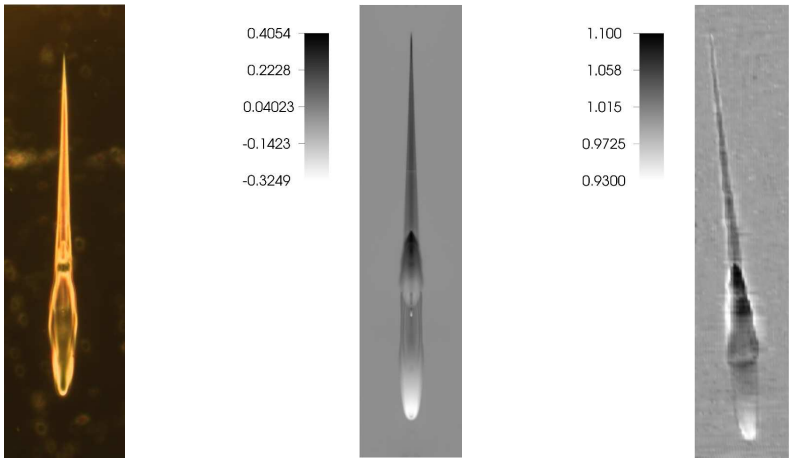

Fig. 4. (a) Photography of Δn. (b) Δn measurement according to quantitative phase imaging technique and Abel inversion [35] (see text). (c) Integrated intensity of the Raman spectra.

#172819 - $15.00 USD Received 18 Jul 2012; revised 15 Oct 2012; accepted 20 Oct 2012; published 12 Nov 2012

fication. The density of $\alpha-$ and $\beta-Ga_2S_3$ (2/3 of triclusters: 3.67-3.69 g·cm^{-3}, 4.70×10^{-2} atoms Å^{-3}) is significantly higher (+25%) compared to low temperature GeS_2 (CS-$GeS_{4/2}$: 2.99 g·cm^{-3}, 3.94×10^{-2} atoms Å^{-3}) or high temperature GeS_2 (CS-$GeS_{4/2}$ and ES-$GeS_{4/2}$: 2.89-2.94 g·cm^{-3}, 3.87×10^{-2} atoms Å^{-3}).

The question arises why the regions with negative Δn and having higher triclusters population compared to the non-irradiated glass, exhibit lower number density. In silica glass, such difference in the Δn sign between the head and the tail has already been observed [36, 37]. The negative Δn sign is associated with the formation of nanoporous region [37] located where the density of electron generated inside the laser filament, is the highest [38]. In $80\,GeS_2-20\,Ga_2S_3$, free carrier accumulation effect due to the high repetition rate of the laser is dominating over the heat accumulation [13, 39]. Correspondingly, we can assume that the negative Δn region is also due to the formation of nanopores arising from Coulombian micro-explosions.

4. Conclusion

A 2D μ-Raman analysis of refractive index variation of $80\,GeS_2-20\,Ga_2S_3$ glass due to femtosecond laser filament has been carried out. This study evidences the reordering of chemical bonds from S_3Ga-GaS_3 ethane like group into triclusters of $\left[GaS_{1/3}S_{3/p}\right]_3$. We also note the decrease of the CS- and ES-$GeS_{4/2}$ tetrahedra population leading to the formation of mixed triclusters $\left[TS_{1/3}S_{3/p}\right]_3$, where T = Ga and/or Ge.

This structural modification is uniform over the irradiated zone whereas Δn reverses its sign between the head and the tail of the structure. Positive Δn in the tail is shown to be due to the higher efficiency of the tricluster tetrahedral packing leading a higher density and number density. Where the free carrier density generated during laser filamentation is high enough to induce Coulombian micro-explosion, the formation of nanovoids leads to negative Δn.

The obtained Raman results show that gallium is a key element for photo-inscription in Ga-containing chalcogenide glasses caused by its labile coordination simplifying the formation of triclusters and ethane-like units as well as a favourable conversion of a loose network organisation into a dense spatial arrangement.

Acknowledgments

We are very grateful to Dr. Laurent Calvez from Université de Rennes 1 for the sample preparation. The Laboratoire de Physico-Chimie de l'Atmosphère participates in the Institut de Recherche en ENvironnement Industriel (IRENI) which is financed by the Communauté Urbaine de Dunkerque, the Région Nord Pas-de-Calais, the Ministère de l'Enseignement Supérieur et de la Recherche, the CNRS and European funds (ERDF). This work was also supported by the European Commission within the framework of the Interreg IVA-2Seas (CleanTech project) programme.

#172819 - $15.00 USD Received 18 Jul 2012; revised 15 Oct 2012; accepted 20 Oct 2012; published 12 Nov 2012